

# Thermomechanical description of shape memory alloys using the preisach model

Thiago Q Alves<sup>1</sup>, Vanderson M Dornelas<sup>1</sup> , Sergio A Oliveira<sup>2</sup> and Marcelo A Savi<sup>1,\*</sup> 

<sup>1</sup> Center for Nonlinear Mechanics, COPPE—Mechanical Engineering, Universidade Federal do Rio de Janeiro, PO Box 68.503, 21.941.972 Rio de Janeiro, RJ, Brazil

<sup>2</sup> Department of Mechanical Engineering, CEFET/RJ—Centro Federal de Educação Tecnológica Celso Suckow da Fonseca, 20.271.110 Rio de Janeiro, RJ, Brazil

E-mail: [savi@mecanica.coppe.ufrj.br](mailto:savi@mecanica.coppe.ufrj.br)

Received 13 September 2023, revised 27 October 2023

Accepted for publication 30 January 2024

Published 12 February 2024



CrossMark

## Abstract

Shape memory alloys (SMAs) are adaptive materials that exhibit complex thermomechanical behaviors due to multiphysics coupling. The thermomechanical modeling of SMAs is a complex task due to several phenomena involved, and the Preisach model is an interesting alternative to describe the SMA hysteretic behavior based on experimental data. This paper deals with the description of the thermomechanical behavior of SMA using the Preisach model. Experimental tests are performed considering NiTi pseudoelastic wires subjected to different load conditions, establishing reference cases. Afterward, the Preisach model is employed to describe the SMA behavior. Numerical simulations are carried out and compared with the experimental data showing a good agreement. Other experimental data available in the literature are employed to investigate different macroscopic behaviors related to SMAs, including strain-temperature relations of wires and force-displacement relations of springs. Results show that the model is able to describe the thermomechanical behavior of SMAs, being in close agreement with experimental data. Preisach model has advantages such as a simple numerical implementation when compared to phenomenological and thermodynamic-based models, being an interesting approach useful for a wide range of applications that include different macroscopic behaviors.

Keywords: shape memory alloys, hysteresis, preisach model, everett function, experimental, numerical simulations

## 1. Introduction

Shape memory alloys (SMAs) belong to the class of smart materials that have a series of complex thermomechanical behaviors, including shape memory effect, pseudoelasticity, phase transformation due to temperature variation, internal subloops due to incomplete phase transformation, and tension-compression asymmetry [1–3]. The remarkable properties related to SMAs are due to solid-solid martensitic phase transformations and hysteretic behavior is the essential point of these complex phenomena involved.

These materials have a significant potential for applications in different areas such as automotive, biomedical, civil engineering, oil and gas, robotics, and aerospace fields [4–14]. In addition, due to their capacity to dissipate energy and to recover large deformations during the phase transformation process, the pseudoelastic behavior has a great potential for applications in vibration attenuation that can be used in different mechanical equipment that show large frequency ranges, devices exposed to impact loads, and earthquake structures [2, 15–19].

The development of engineering applications and new devices that use SMAs must be associated with a proper understanding of their thermomechanical behavior. In this regard, SMA modeling is an essential task to be considered, and different approaches can be employed for this aim. In general,

\* Author to whom any correspondence should be addressed.

it can be considered a multiscale description varying from micro to macroscopic levels. The most interesting approach includes the thermodynamic-based models that encompass the phenomenological macroscopic behaviors.

Several constitutive models are proposed to describe the thermomechanical behavior of SMAs. A general review of the main models is discussed by Paiva and Savi [20], Khandelwal and Buravalla [21], Cisse *et al* [22, 23], and Chowdhury [24]. Among these models, it is important to highlight one-dimensional models: Falk [25, 26], Tanaka [27], Brinson [28], Auricchio and Sacco [29], Savi *et al* [30], Paiva *et al* [31], and Adeodato *et al* [32]. For three-dimensional media, it is important to highlight the works developed by Souza *et al* [33], Popov and Lagoudas [34], Auricchio *et al* [35], Oliveira *et al* [36, 37], Chemisky *et al* [38], Phillips *et al* [39], and Dornelas *et al* [40, 41].

Experimental-based or geometric-based models are another alternative that avoids the definition of material properties, presenting a generalist perspective that allows the description of different phenomena including magnetic, ferroelectric, optical, superconducting, adsorption, economic, and mechanical. Usually called hysteresis models, they are essentially based on experimental data, being adjusted by geometrical perspectives and with simplicity as an advantage.

According to Khandelwal and Buravalla [21], there are two main approaches in the literature using hysteresis models, originally employed to describe magnetic materials: the Preisach model and the Duhem–Madelung model. The Preisach model promotes the integration of the material response considering two fixed states, which represent the type of transformation that occurs. On the other hand, the Duhem–Madelung model represents the hysteresis through differential equations considering two differential operators to represent the loading and unloading processes. In addition, Bouc–Wen, Prandtl–Ishlinskii, and Krasnosel’skii–Pokrovkii models are also employed to describe hysteresis, being explored by several researchers such as Kuhnen [42], Al Janaideh *et al* [43, 44], and Zakerzadeh and Sayyaadi [45].

The classical Preisach model [46] was proposed in 1935 to represent the ferromagnetic behavior [47]. Only in the 1970s, a new interpretation of the Preisach model was presented by Krasnosel’skii [48], being employed for a general representation of the hysteretic behavior. In brief, this model describes the hysteresis from the superposition of operators in a triangular domain, defined in an abstract space. The use of the Preisach model to describe smart material hysteresis has been explored in several works developed in the last few years. In this regard, piezoelectric materials were discussed by Song *et al* [49], Dong *et al* [50], and Xue *et al* [51]; while magnetostrictive materials were treated by Adly *et al* [52], Davino *et al* [53], Li *et al* [54], and Trapanese *et al* [55].

Concerning SMAs, it should be highlighted the work of Smith [56] that presented a discussion of the use of the Preisach model for SMA modeling. Hughes and Wen [57, 58] listed the microstructural mechanisms that promote hysteresis in SMAs and piezoelectric materials, identifying similarities between these materials and ferromagnetic materials. Gorbet

*et al* [59] developed numerical-experimental comparisons considering the Preisach model, and experimental results obtained through an actuator composed by SMA wires. Results showed that the model responses are in good agreement with experimental data attesting to the model’s ability to represent the SMA phenomena.

Mayergoyz [48, 60] developed a new formulation of the Preisach model using Everett functions, built from experimental data. This approach facilitates the correlation with experimental data, simplifying the numerical implementation. Khan and Lagoudas [61] employed the Preisach model to simulate the response of pseudoelastic SMA springs used in dynamical vibration absorbers using the formulation proposed by Mayergoyz [48]. Rao and Srinivasa [62] developed a hybrid model based on the work proposed by Doraiswamy *et al* [63] to simulate the pseudoelastic response for SMA wires and springs. The model combined thermodynamics principles and Preisach model to separate the thermoelastic and dissipative responses. Rao *et al* [64] investigated the response of pseudoelastic SMA wires subjected to torsional loads with subloops. Numerical-experimental comparisons using the model proposed by Rao and Srinivasa [62] were performed, showing that the thermodynamic approach has a broader predictive capacity when compared to the classical Preisach model. In addition, other studies are available considering the Preisach model to describe the characteristics of hysteresis in SMAs, for instance: Ktena *et al* [65], Matsuzaki *et al* [66]; Liang *et al* [67], Rao and Srinivasa [68], and Chen *et al* [69].

This paper investigates the use of the Preisach model for the thermomechanical description of SMAs, considering different macroscopic behaviors. The classic Preisach model is reviewed and an alternative procedure using the Everett function built from experimental data is discussed. Experimental tensile tests are carried out to define reference cases. Numerical simulations are carried out, evaluating the model capability to describe the SMA thermomechanical behavior, including internal subloops. Results showed that the model responses are in close agreement with experimental data. Afterward, the model is applied to distinct macroscopic behaviors including stress–strain and strain–temperature curves of wires and force–displacement curves of helical springs. These results show broader possibilities associated with the SMA description. The Preisach model showed to be an interesting approach for the description of a wide range of applications, being useful for applications where previous tests are not available to determine model parameters.

After this introduction, this work is structured as follows. Section 2 presents an experimental investigation considering pseudoelastic wires subjected to different load conditions to evaluate the pseudoelasticity and internal subloops due to incomplete phase transformation. Section 3 presents the mathematical fundamentals of the Preisach model and a discussion of the Everett function showing its construction from experimental data. Numerical simulations and their comparison with the experimental data are presented in section 4. Initially, a comparison with reference experimental data is performed

and afterward, other results from the literature are employed considering different macroscopic behaviors including SMA springs. The conclusions are presented in section 5.

## 2. Experimental investigation

This section presents the main macroscopic characteristics of the thermomechanical behavior of SMAs through experimental observations. The experimental tests are performed using a pseudoelastic Ni56Ti44 (wt.%) circular section wire in an as-received condition, with a diameter of 1.30 mm manufactured by Sandinox biomaterials. Quasi-static tensile tests are performed using an electro-mechanical testing machine, Instron 5882, employing a 30 kN static load cell and strain measurement based on displacement with a gage length of 100 mm. For more details about the experimental setup, see Dornelas *et al* [41].

The specimen is subjected to a training process through a quasi-static cyclic tensile test with a peak stress of 900 MPa and a stress rate of  $180 \text{ MPa min}^{-1}$ . Figure 1(a) shows the stress–strain curves obtained from 50 cycles, highlighting the first and last cycles during the training process. Figure 1(b) presents the evolution of the strain over the cycles, observing the stabilization after approximately thirty cycles. This stabilization is associated with the transformation induced plasticity (TRIP), being essential for the use of SMAs in their various applications, allowing response repeatability. It is noticeable that the stabilization process promotes a reduction of the SMA functional properties, such as the size of the hysteresis loop and the strains where phase transformations start and finish [37].

### 2.1. Cyclic tests

After the training procedure, the pseudoelastic behavior is exploited considering different thermomechanical loads by applying prescribed strain. Initially, a test considering nine cycles, with maximum strain varying between 1% (in the first cycle) and 9% (in the last cycle) and minimum strain close to zero, with a loading rate of  $0.5\% \text{ min}^{-1}$  is of concern. Figure 2(a) shows the test loading history while figure 2(b) presents the corresponding stress–strain curve. Note that the SMA sample does not present phase transformation during the first cycle (a maximum strain of 1%), showing incomplete phase transformation between cycles two and six. From the seventh cycle, the sample presents complete phase transformation associated with the external loop.

Two other experimental tests are presented in the sequel defining different internal subloops. Figure 3(a) shows a mechanical loading at a strain rate of  $0.5\% \text{ min}^{-1}$ . Figure 3(b) presents the stress–strain curve showing an external hysteresis loop, an envelope of the two internal subloops due to incomplete phase transformation. A new loading process is presented in figure 4(a) considering a strain rate of  $1\% \text{ min}^{-1}$ . Figure 4(b) presents the stress–strain curve where it is observed a subloop due to the incomplete phase transformation and an external loop that represents the complete transformation.

## 3. Mathematical model

This section presents the description of the SMA thermo-mechanical behavior through the Preisach model. Initially, the Preisach model is presented and afterward, the Everett surface is discussed showing its construction from experimental data.

### 3.1. Preisach model

The Preisach model is a generalist description that can be employed for multiphysics hysteretic phenomena. The model is built from elementary operators defined in an abstract space, called Preisach hysteresis operators, which correspond to two states, such as the SMA austenitic and martensitic phases.

The Preisach operator,  $\hat{\gamma}_{\alpha\beta}$ , is combined in rectangular loops in an input-output diagram, representing a hysteretic behavior [48]. In addition, this operator is associated with abstract variables,  $\alpha$  and  $\beta$ , respectively associated with two directions of transformation, as illustrated in figure 5 which shows the operator as a function of some input (such as the strain,  $\varepsilon$ ). Therefore, when the input is increased, the ascending branch *a-b-c-d-e* is followed. On the other hand, when the input decreases, the descending branch *e-d-f-b-a* is followed.

In this regard, a generic hysteresis curve such as stress–strain ( $\sigma - \varepsilon$ ), force–displacement ( $f - u$ ), or strain–temperature ( $\varepsilon - T$ ) can be represented as a sequence of elementary transformations, expressed by the superposition of elementary operations defined by hysteresis operators. Therefore, it is assumed, without loss of generality, a hysteresis curve of stress (output), as a function of strain (input), which is expressed as follows, assuming that  $\alpha \geq \beta$  since hysteresis is a dissipative phenomenon:

$$\sigma(\varepsilon) = \hat{\Gamma}\varepsilon = \int_{\alpha_0}^{\alpha_n} \int_{\beta_0}^{\beta_n} \mu(\alpha, \beta) \hat{\gamma}_{\alpha\beta} d\alpha d\beta \quad (1)$$

where  $\mu(\alpha, \beta)$  is the Preisach function and  $\hat{\Gamma}$  represents the concise notation of the Preisach hysteresis operator [48]. In addition,  $\alpha_0$  and  $\beta_0$  represent the smallest switching values and  $\alpha_n$  and  $\beta_n$  represent the highest switching values.

Mayergoyz [48] proposed a different approach by replacing the integration by a summation and the Preisach function by the Everett function ( $F$ ), built from experimental data. This procedure mitigates amplification errors and simplifies the numerical implementation [61]. Therefore equation (1) can be rewritten as a summation of Everett functions, as follows:

$$\sigma(\varepsilon) = \sum_{k=1}^n [F(\alpha_k, \beta_{k-1}) - F(\alpha_k, \beta_k)]. \quad (2)$$

On this basis, the SMA hysteretic behavior can be described using the Preisach model following the structure illustrated in figure 6. Experimental data are used to build the Everett function that allows one to establish the relationship with the Preisach space.

In this regard, numerical simulations can be considered as a geometrical-based approach adjustment from experimental

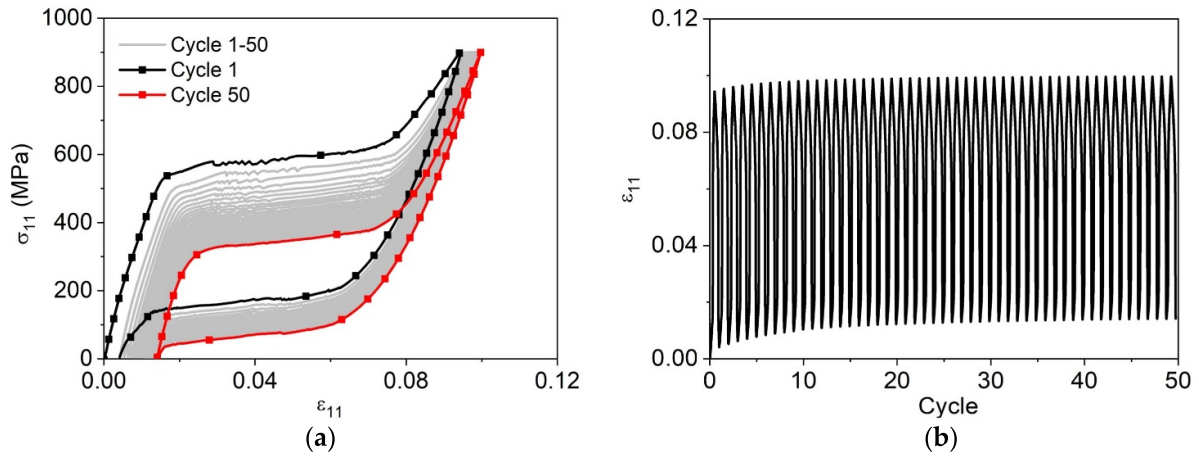


**Figure 1.** Quasi-static tensile tests of a pseudoelastic NiTi wire, training procedure. (a) Cyclic stress–strain response presenting 50 cycles; (b) TRIP strain stabilization throughout the cycles.

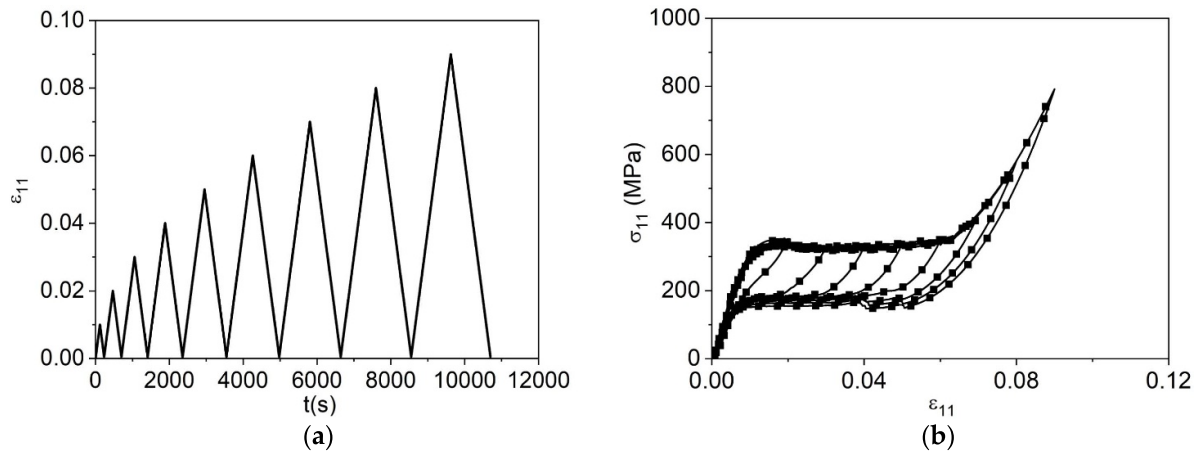


**Figure 2.** Quasi-static tensile tests of a pseudoelastic NiTi wire with a strain rate of  $0.5\% \text{ min}^{-1}$ . (a) Loading history; (b) stress–strain curve.

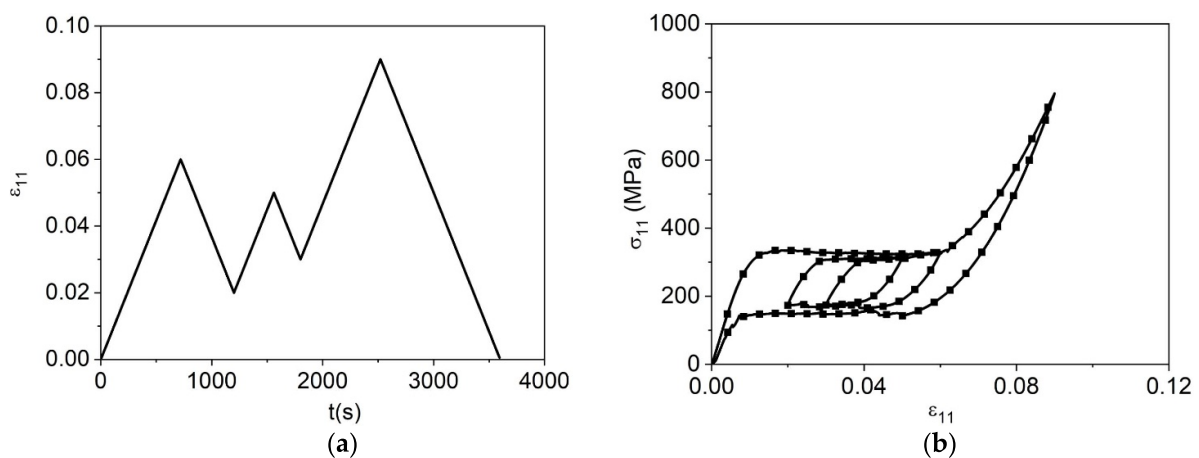


**Figure 3.** Quasi-static tensile tests of a pseudoelastic NiTi wire with a strain rate of  $0.5\% \text{ min}^{-1}$ . (a) Loading history; (b) stress–strain curve considering two internal subloops.

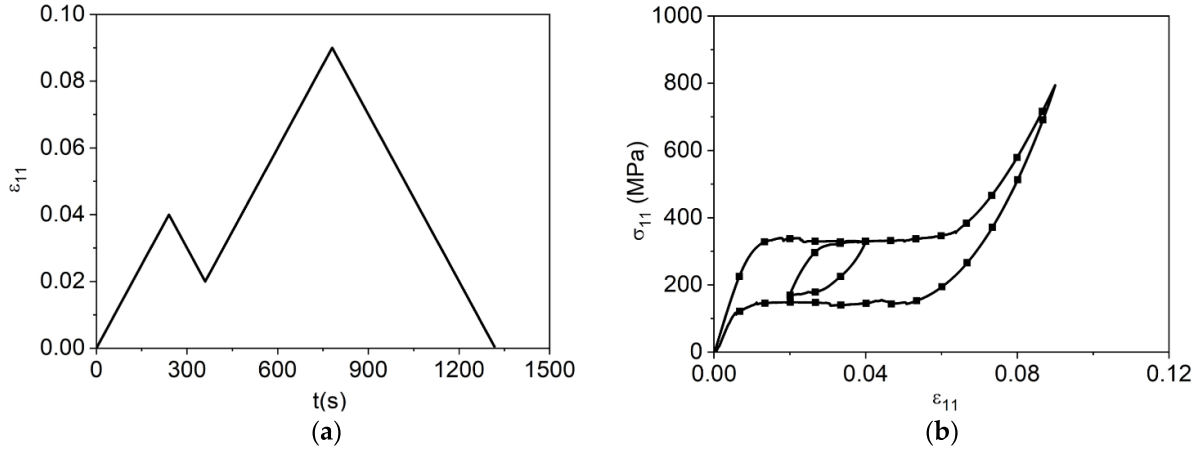


**Figure 4.** Quasi-static tensile tests of a pseudoelastic NiTi wire. Loading history, and stress–strain curves with a strain rate of  $1\% \text{ min}^{-1}$ . (a) Loading history; (b) stress–strain curve considering one internal subloop.

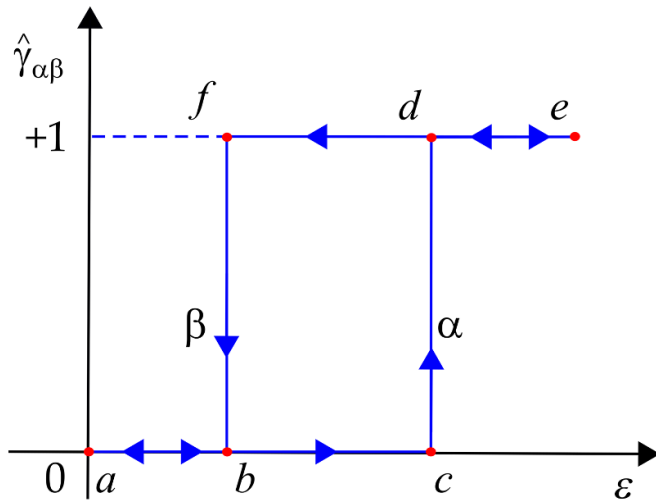


**Figure 5.** Definition of the Preisach hysteresis operator.

data. In essence, experimental data provide a set of points that defines the Everett surface that is employed by the Preisach approach to generate a synthetic thermomechanical behavior SMAs.

**3.1.1. Geometric interpretation.** The geometric interpretation of the Preisach triangle is shown in figure 7 considering a stress–strain curve. In this regard, the triangular representation is built by considering that the upper limit of the  $\alpha$  coordinate corresponds to the maximum strain value. On the other hand, the lower limit of the  $\beta$  coordinate corresponds to the minimum strain value. The line  $\alpha = \beta$  is added to these limits, considering  $\alpha \geq \beta$ . In addition, the stress value at any point in the hysteresis region can be obtained from the appropriate choice of  $\alpha - \beta$  coordinates.

The representation of the hysteresis evolution in the Preisach triangle is schematically showed in figure 8. In general, an increase of the value of  $\varepsilon$  ( $\dot{\varepsilon} > 0$ ) provides a change

in the  $\alpha$ -axis while a decrease ( $\dot{\varepsilon} < 0$ ) changes the  $\beta$ -axis. Furthermore, an increase of the value of  $\varepsilon$  implies summing a value of the Everett function in equation (2) while a decrease of  $\varepsilon$  implies subtraction.

On this basis, at the initial time,  $t_0$ , the material has a strain  $\varepsilon_0$  at the beginning of the hysteresis region, corresponding to the coordinates in the Preisach plane  $(\alpha_0, \beta_0) = (\varepsilon_0, \varepsilon_0)$ . After identifying the coordinates in the Preisach plane, the Everett surface is calculated and applied in equation (2) obtaining the stress value,  $\sigma(\varepsilon) = F(\alpha_0, \beta_0)$ . Afterward, the strain increases and reaches the value  $\varepsilon_1$ . The variation of strain is represented by the grayscale color in the Preisach triangle. The division is performed by the line  $\alpha = \varepsilon$ , which moves upward as  $\varepsilon$  increases until it reaches  $\varepsilon_1$ . Since this is the first variation in the  $\alpha$  coordinate, it is labeled with the index 1. Thus, the new coordinates in the Preisach plane are  $(\alpha_1, \beta_0) = (\varepsilon_1, \varepsilon_0)$ , and the Everett function is determined. By applying equation (2), the value of the stress is calculated as  $\sigma(\varepsilon) = F(\alpha_1, \beta_0)$ . The Preisach model has the property of storing only the extreme points of the  $\alpha$  and  $\beta$  coordinates (wiping-out property) [48, 60]. Therefore, an increment in the  $\alpha$  coordinate promotes the replacement of  $\alpha_0$  by  $\alpha_1$  resulting in the replacement of the Everett function  $F(\alpha_0, \beta_0)$  by  $F(\alpha_1, \beta_0)$ .

In the sequence, it is assumed that the input variable decreases continuously until it reaches a minimum value  $\varepsilon_2$ . The boundary line showed in the Preisach triangle has two straight lines: one horizontal and one vertical. The vertical line moves until it reaches  $\beta = \varepsilon_2$ . Once again, applying the coordinates obtained in the Preisach plane  $(\alpha_1, \beta_1) = (\varepsilon_1, \varepsilon_2)$ , the Everett function is determined. Therefore, the stress value can be obtained through equation (2):  $\sigma(\varepsilon) = F(\alpha_1, \beta_0) - F(\alpha_1, \beta_1)$ . This result illustrates another property of the Preisach model that consists of accumulating the values obtained in previous operations. Note that  $\sigma(\varepsilon)$  is composed by a portion obtained in the previous step accumulated with the result obtained in the current step.

By considering new inputs up to  $\varepsilon_5$ , the evolution of the coordinates in the Preisach plane is obtained, and

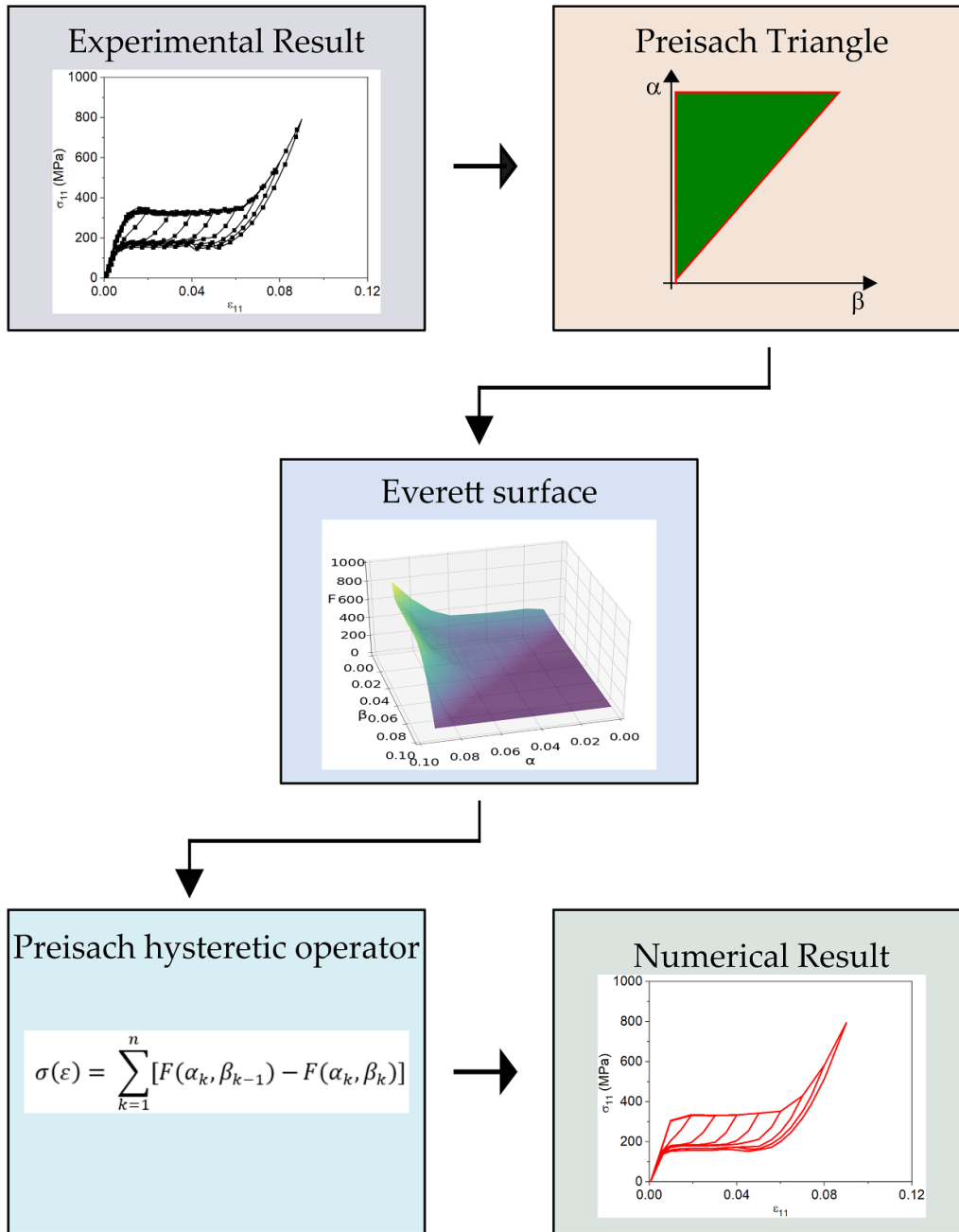


**Figure 6.** Schematic picture of the SMA description using the Preisach model.

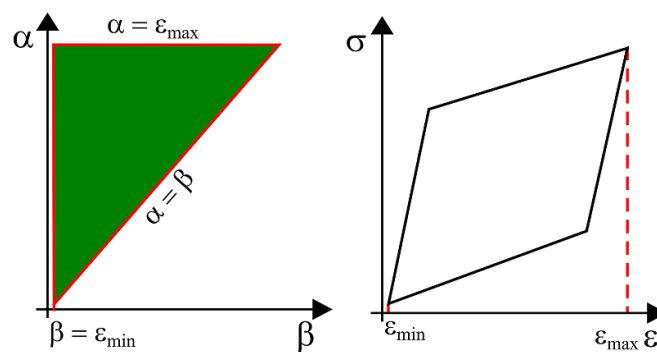


**Figure 7.** Preisach triangle and the associated hysteresis in stress–strain curve.

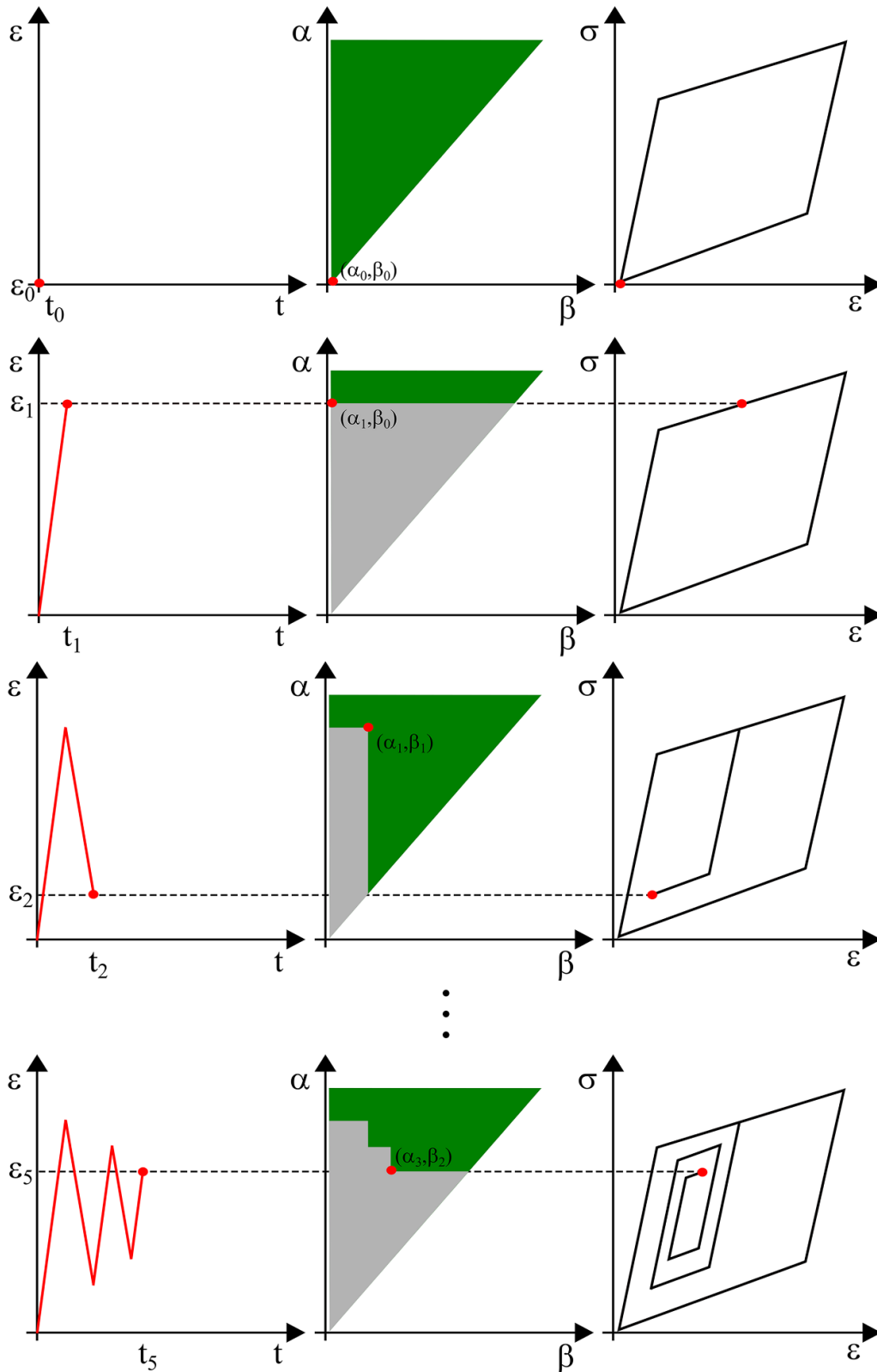


**Figure 8.** Evolution of the Preisach triangle and the associated hysteresis obtained from a prescribed strain.

these coordinates are employed in the calculation of the Everett surface. Equation (2) allows the determination of the stress values. Therefore, an increase in the strain value promotes a variation in the  $\alpha$  -axis and an accumulation

of a positive portion of the Everett function. On the other hand, a decrease in the strain value implies a variation in the  $\beta$  -axis and a negative portion of the Everett function.

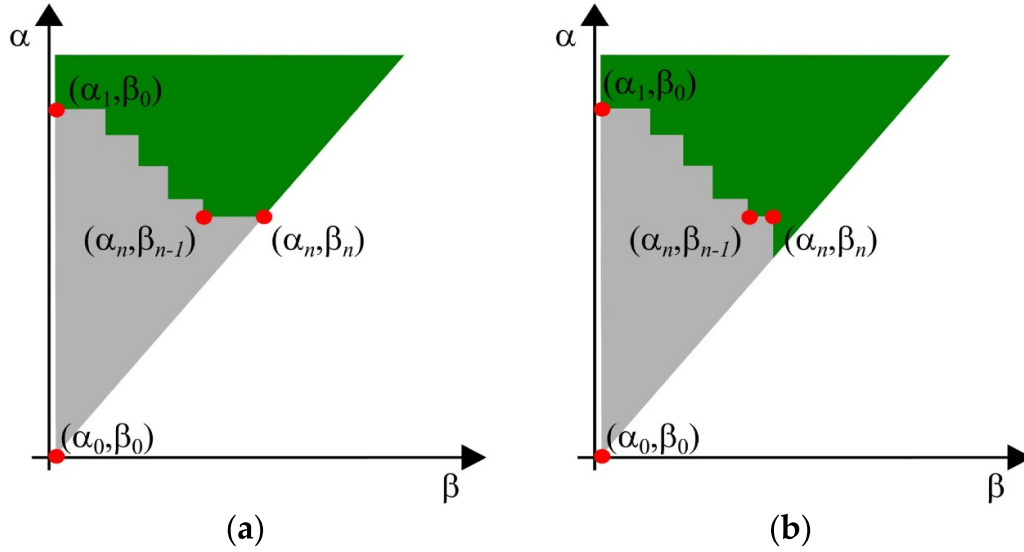


**Figure 9.** Trapezoid coordinates on the boundary line. (a) Increasing input (b) decreasing input.

In general, expressions for stress as a function of  $F(\alpha_n, \beta_n)$  can be divided into two cases based on strain increase or decrease. For the strain increase ( $\dot{\varepsilon} > 0$ ), showed in figure 9(a), the last change in  $\varepsilon$  corresponds to a value in the  $\alpha$  coordinate, which segment is a horizontal line. Therefore, equation (2) can be rewritten as follows:

$$\sigma(\varepsilon) = \sum_{k=1}^{n-1} [F(\alpha_k, \beta_{k-1}) - F(\alpha_k, \beta_k)] + F(\varepsilon_n, \beta_{n-1}). \quad (3)$$

On the other hand, for a decreasing strain ( $\dot{\varepsilon} < 0$ ), showed in figure 9(b), the final segment is a vertical line, and the last change in  $\varepsilon$  corresponds to a value in the  $\beta$  coordinate. Therefore, equation (2) can be rewritten as:

$$\sigma(\varepsilon) = \sum_{k=1}^{n-1} [F(\alpha_k, \beta_{k-1}) - F(\alpha_k, \beta_k)] + F(\alpha_n, \beta_{n-1}) - F(\alpha_n, \varepsilon_n). \quad (4)$$

### 3.2. Everett function

The Everett function is a surface on  $\mathbb{R}^3$ , built from experimental data and establishing a connection with the Preisach domain. The Everett surface is defined by the number of experimental points necessary for the description of the hysteretic behavior, given through the coordinate points  $(\alpha, \beta, F)$  associated with the Preisach triangle. An interpolation can be employed to define the Everett function.

The construction of the Everett surface is now in focus using an experimental stress–strain curve as example. Figure 10 illustrates the construction of the Everett surface by dividing the stress–strain space into nine regions. The experimental points identified in the stress–strain curve are highlighted by red dots, showed in figure 10(a). Figure 10(b) presents the Preisach triangle, showing that each experimental point has an equivalence in the Preisach triangle space. These

experimental points are represented as solid points, while the gray points represent the external points to the Preisach triangle. Finally, figure 10(c) shows the Everett surface obtained by mapping the experimental points. It is observed that the Everett function appears as an envelope of the region of the Preisach triangle (solid red dots).

On this basis, a procedure to determine the coordinate points  $(\alpha, \beta, F)$ , is presented in the sequel:

1. Select the experimental data.
2. Divide the hysteresis region into an appropriate number of divisions using vertical lines.
3. Identify the experimental points obtained by the intersection between the vertical lines and the experimental data.
4. Identify the experimental strain values to obtain  $\alpha$  and  $\beta$  values.
5. Build the  $H_{\alpha\beta}$  stress matrix, which defines the third coordinate to obtain the Everett surface.
6. Build the Everett function by two-dimensional linear interpolation.

To illustrate the procedure for obtaining the  $H_{\alpha\beta}$  matrix, consider the experimental data showed in figure 10(a) with nine divisions of the stress–strain space. From lines  $\varepsilon_{0 \rightarrow 9}$ , nineteen experimental points are obtained as showed in table 1. It is observed that points 1 and 19 are coincident, and therefore, present the same strain and stress values. There is a correspondence between the stress–strain space and the Preisach domain and therefore, it is necessary to map the Preisach plane for ten lines  $\varepsilon_{0 \rightarrow 9}$ , considering  $\alpha_i = \beta_i = \varepsilon_i$  ( $i = 0, 1, 2, \dots, 9$ ) as illustrated in figure 10(b).

The construction of  $H_{\alpha\beta}$  matrix is illustrated in table 2, which allows one to calculate coordinate  $F$ . The values of the first line are found by subtracting the smallest stress value of the experimental points of the austenite  $\rightarrow$  martensite transformation ( $\sigma_1$ ) from the stress values of each experimental point of this same transformation ( $\sigma_1 - \sigma_{10}$ ). On

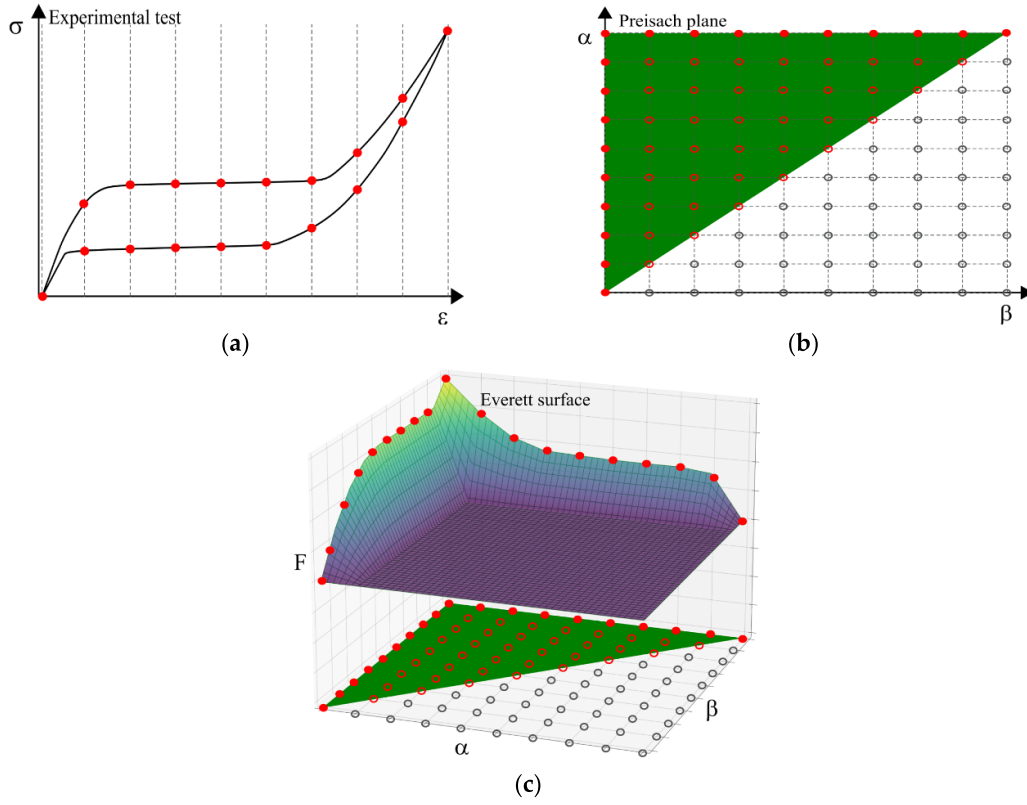


**Figure 10.** Everett surface construction. (a) Experimental points mapped from a division of the hysteresis region; (b) associated Preisach triangle considering the mesh obtained from the proposed division; (c) Everett surface obtained.

**Table 1.** Experimental points obtained by dividing the stress–strain space into nine regions.

Experimental point	Strain	Stress
1	$\varepsilon_0$	$\sigma_1$
2	$\varepsilon_1$	$\sigma_2$
$\vdots$	$\vdots$	$\vdots$
9	$\varepsilon_8$	$\sigma_9$
10	$\varepsilon_9$	$\sigma_{10}$
11	$\varepsilon_8$	$\sigma_{11}$
$\vdots$	$\vdots$	$\vdots$
18	$\varepsilon_1$	$\sigma_{18}$
19	$\varepsilon_0$	$\sigma_{19} = \sigma_1$

**Table 2.** Determination of the  $H_{\alpha\beta}$  matrix.

	$\alpha_0$	$\alpha_1$	$\dots$	$\alpha_8$	$\alpha_9$
$\beta_0$	$\sigma_1 - \sigma_1$	$\sigma_2 - \sigma_1$	$\dots$	$\sigma_9 - \sigma_1$	$\sigma_{10} - \sigma_1$
$\beta_1$	0	0	$\dots$	0	$\sigma_{10} - \sigma_{18}$
$\vdots$	$\vdots$	$\vdots$	$\ddots$	$\vdots$	$\vdots$
$\beta_8$	0	0	$\dots$	0	$\sigma_{10} - \sigma_{11}$
$\beta_9$	0	0	$\dots$	0	$\sigma_{10} - \sigma_{10}$

the other hand, the values in the last column are obtained by subtracting the highest stress value of the experimental points of the martensite  $\rightarrow$  austenite transformation ( $\sigma_{10}$ ) from the stress values of each experimental point of this transformation ( $\sigma_{19} - \sigma_{10}$ ). After obtaining the  $H_{\alpha\beta}$  matrix,

a linear interpolation is performed and the Everett surface is obtained, as showed in figure 10(c). Based on the considered experimental points, the matrix  $H_{\alpha\beta}$  has only the first row and the last column with non-vanishing values.

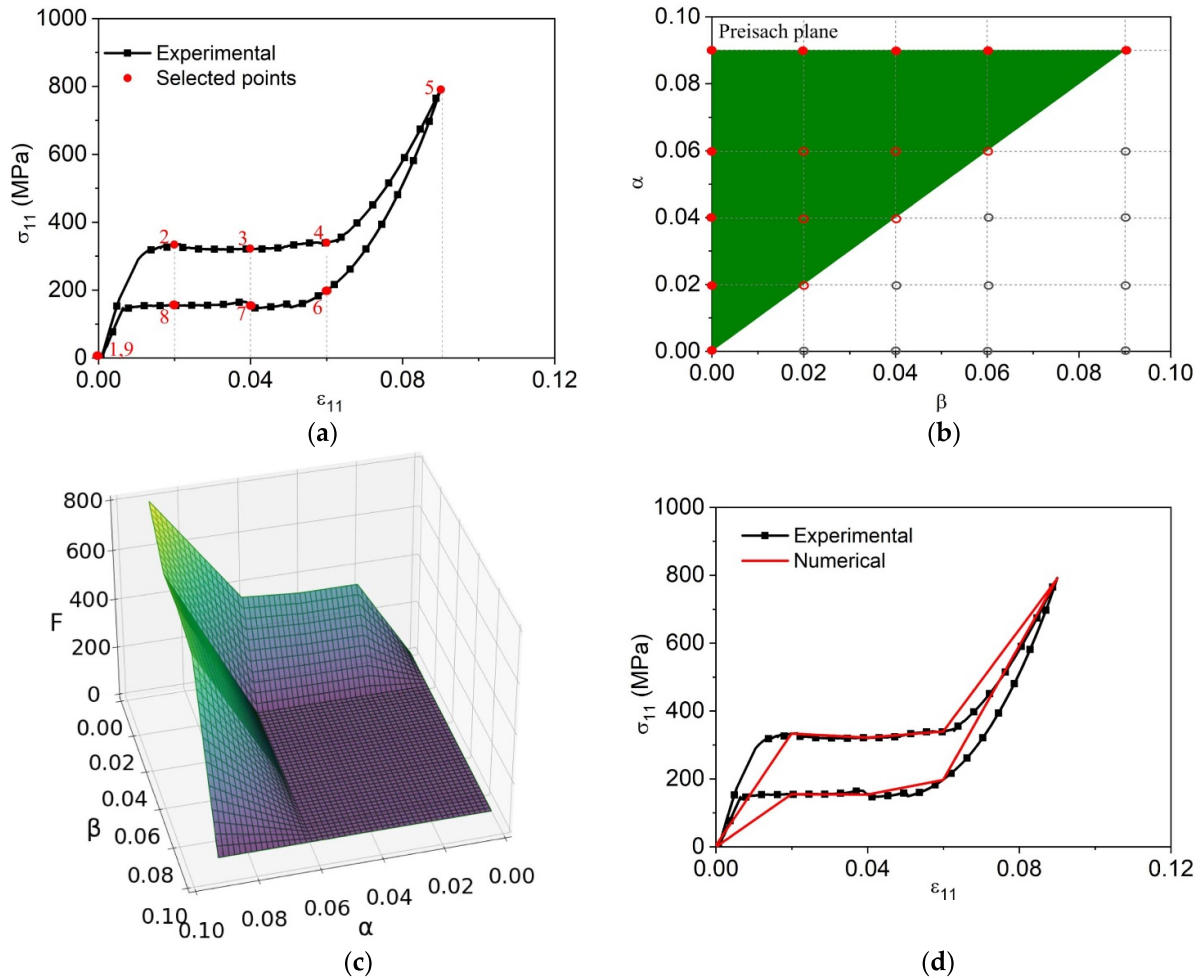


**Figure 11.** Numerical results obtained from the Preisach model considering four regions in the stress–strain space of an experimental result. (a) Selected points on the experimental curve used in the numerical implementation; (b) associated Preisach triangle; (c) Everett surface; (d) numerical-experimental comparison.

## 4. Numerical simulations

Numerical simulations are now carried out in order to show the Preisach model's capabilities to capture the thermomechanical behaviors of SMAs. In this regard, comparisons between numerical and experimental results are presented. Initially, a discussion on the construction of the Everett surface and the numerical representation of the mechanical behavior of the material is presented. Next, the numerical-experimental comparisons are shown. Finally, other macroscopic phenomena related to SMAs are analyzed considering experimental results available in the literature.

### 4.1. Everett function

The proper definition of the Everett surface is essential for the description of the thermomechanical behavior of SMAs through the Preisach model. In this regard, the procedure discussed in the previous section is considered to evaluate the relationship between the number of experimental points necessary for the construction of the Everett surface and the

numerical results. Therefore, it is possible to estimate the minimum number of divisions of the experimental space necessary for a correct representation of the material behavior.

This analysis is developed from the experimental results discussed in section 2.1, figure 2, considering only the external loop. Initially, consider the stress–strain space divided into four regions, associated with nine experimental points, as showed in figure 11(a). The Preisach triangle associated with the experimental points is illustrated in figure 11(b) while the Everett surface is shown in figure 11(c). The numerical-experimental comparison is shown in figure 11(d) where it is observed a discrepancy between results, demonstrating that the number of experimental points for the construction of the Everett surface is insufficient for the correct description of the pseudoelastic behavior.

A refinement is adopted considering nine divisions in the stress–strain space, which is associated with nineteen experimental points as illustrated in figure 12(a). Figure 12(b) shows the correspondent Preisach triangle and figure 12(c) presents the Everett surface where it is noticeable a smoother surface when compared with the previous case. Since only the external

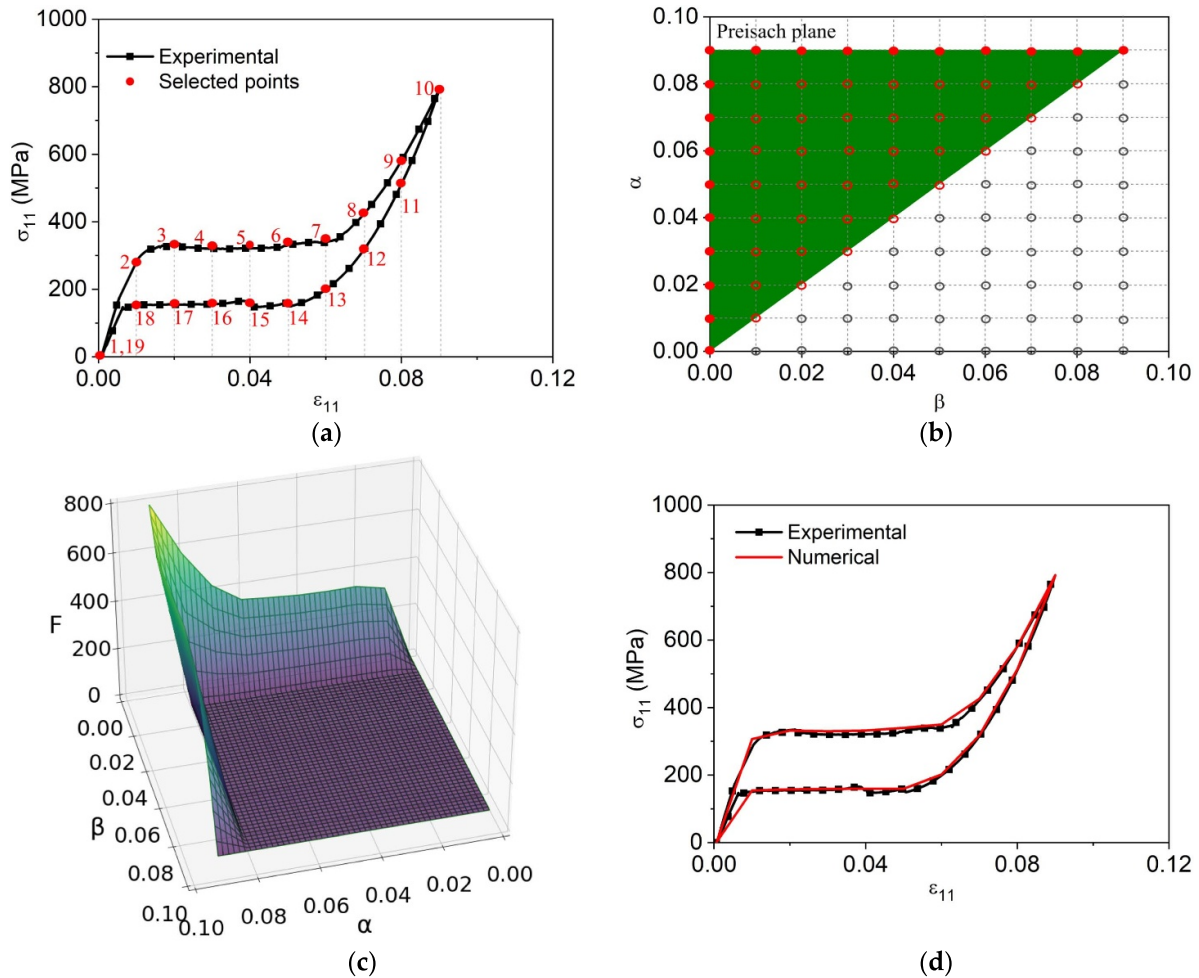


**Figure 12.** Numerical results obtained from the Preisach model considering nine regions in the stress–strain space of an experimental result. (a) Selected points on the experimental curve used in the numerical implementation; (b) associated Preisach triangle; (c) Everett surface; (d) numerical-experimental comparison.

loop is used for both tests, the Everett function is just an envelope of the Preisach triangle. The numerical-experimental comparison is presented in figure 12(d) showing a good agreement with experimental data. Based on that, it is assumed nine divisions as a minimum value for a correct representation of the SMA macroscopic behavior through the Preisach model. This value is greater than the one employed by Del Hoyo [70] where eight divisions were employed to estimate the Everett function to describe several levels of magnetization using the Preisach model.

#### 4.2. Pseudoelastic tests

This section treats the experimental pseudoelastic tests discussed in section 2.1. Initially, the Everett function is estimated considering internal subloops, which map the interior region of the Preisach triangle domain. Figure 13(a) presents the experimental test with nine load cycles with maximum strain varying between 1% and 9% and minimum strain close to zero. Nine partitions in the stress–strain space are adopted and the

experimental points are selected for the construction of the Everett surface. Figure 13(b) shows the Preisach triangle considering selected experimental points. The Everett function is defined in every region of the Preisach triangle as shown in figure 13(c). Figure 13(d) presents the numerical results obtained from the Preisach model, showing that the model captures the general qualitative behavior of the SMA during pseudoelastic loading tests.

Figure 14 highlights the numerical-experimental comparison for different cycles (2, 4, 6, and 9), showing all numerical cycles in the background, in grayscale, to facilitate the visualization. It should be pointed out a good agreement between numerical and experimental results, showing the model's capability to describe the SMA pseudoelastic response. Furthermore, results demonstrate that the use of nine divisions in the experimental stress–strain space is satisfactory for the construction of the Everett function.

Based on the Everett function built for the previous test, two new numerical-experimental comparisons are performed based on the experimental results discussed in section

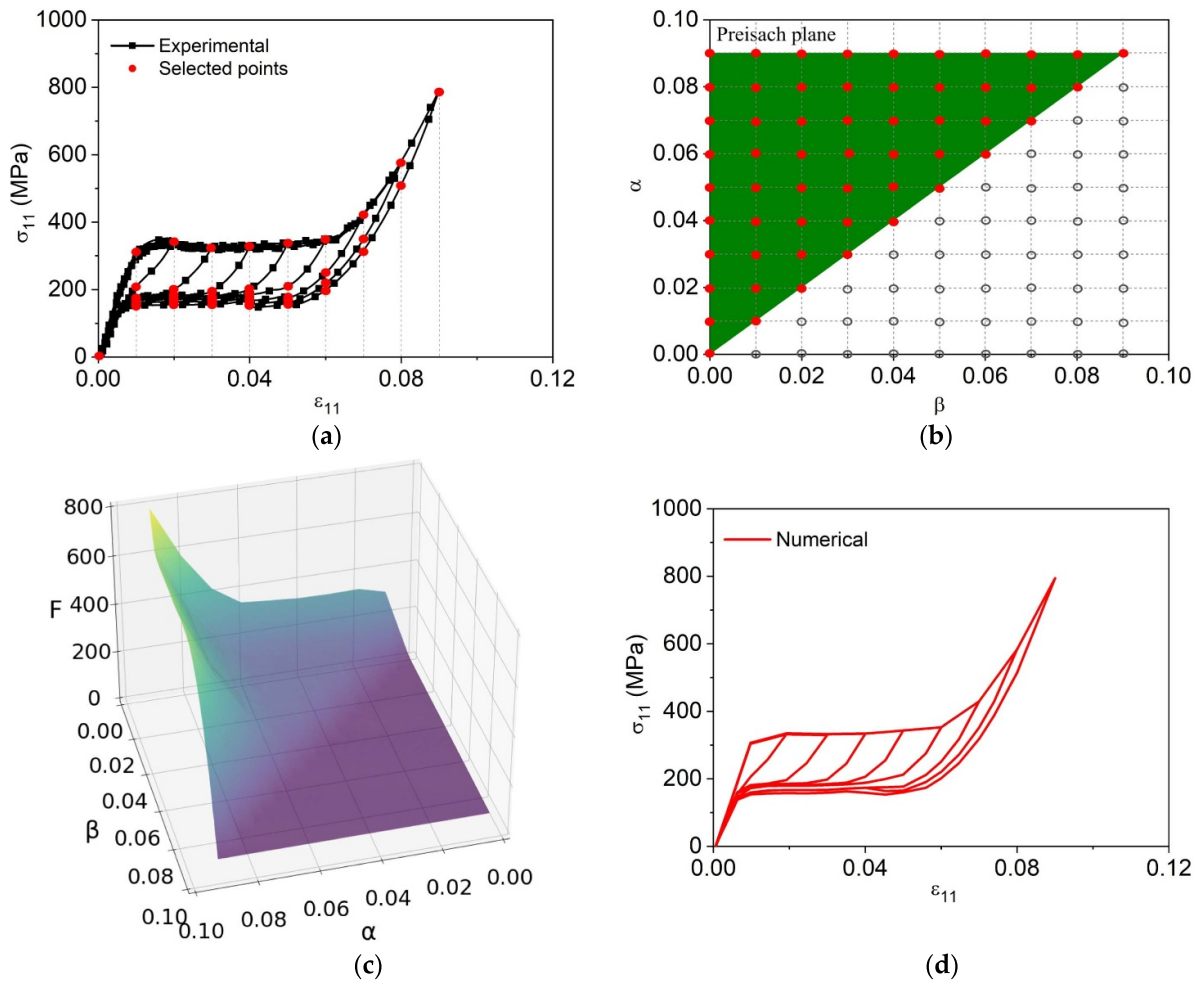


**Figure 13.** Pseudoelastic behavior of a NiTi wire during tensile tests. (a) Selected points on the experimental curve used in the numerical implementation; (b) associated Preisach triangle; (c) Everett surface; (d) numerical result.

2.1. Initially, consider the experimental result presented in figure 15(a) which shows a stress–strain curve with two internal subloops due to incomplete phase transformation. Figure 15(b) shows the numerical–experimental comparison, where it is possible to observe a good agreement between the results. This result shows that two different tests can be described by the same Everett function, which is an interesting property that enlarges the model application.

A new test is in focus considering internal subloops discussed in figure 16(a). Figure 16(b) presents the numerical–experimental comparison, where it is possible to observe a good agreement. Once again, it should be highlighted that the Preisach model is able to reproduce the thermomechanical behavior of SMAs under different loading conditions using the same Everett function. Note that once the Everett function is properly defined from a general experimental test, figure 13(c), the model can reproduce other behaviors associated with SMAs, such as different subloops due to incomplete phase transformations.

#### 4.3. Thermal loadings

The thermomechanical behavior of SMAs due to thermal loadings is now in focus considering the experimental result presented by Qin *et al* [71] as reference. This work studied NiTi wires subjected to different thermal loads, initially in the austenitic phase, at constant stress. Figure 17(a) shows the experimental strain–temperature curve obtained after ten training cycles varying the sample temperature between 367–292 K and the respective selected experimental points. The Everett function is built considering nine divisions, where it is possible to identify the selected experimental points. The temperature is assumed to be the input variable while strain is the output. Since the increase in temperature causes the strain decrease, the Preisach triangle is adjusted considering  $\alpha \leq \beta$  as showed in figure 17(b). Experimental points are related to the external loop and therefore, the Everett function is just the envelope of the Preisach triangle as illustrated in figure 17(c). Figure 17(d) presents the comparison between numerical and

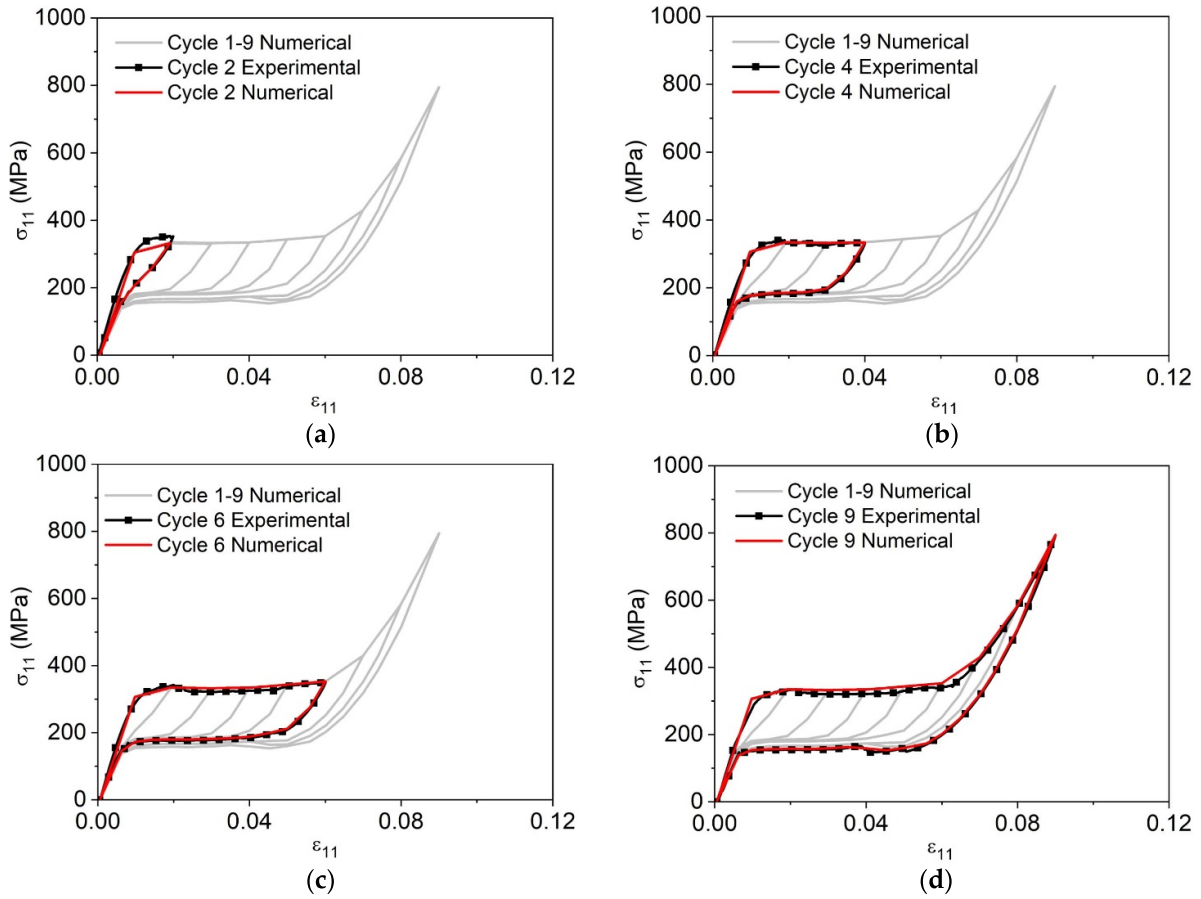


**Figure 14.** Pseudoelastic behavior of a NiTi wire during tensile tests. Numerical-experimental comparative for different cycles. (a) Cycle 2; (b) cycle 4; (c) cycle 6; (d) cycle 9.

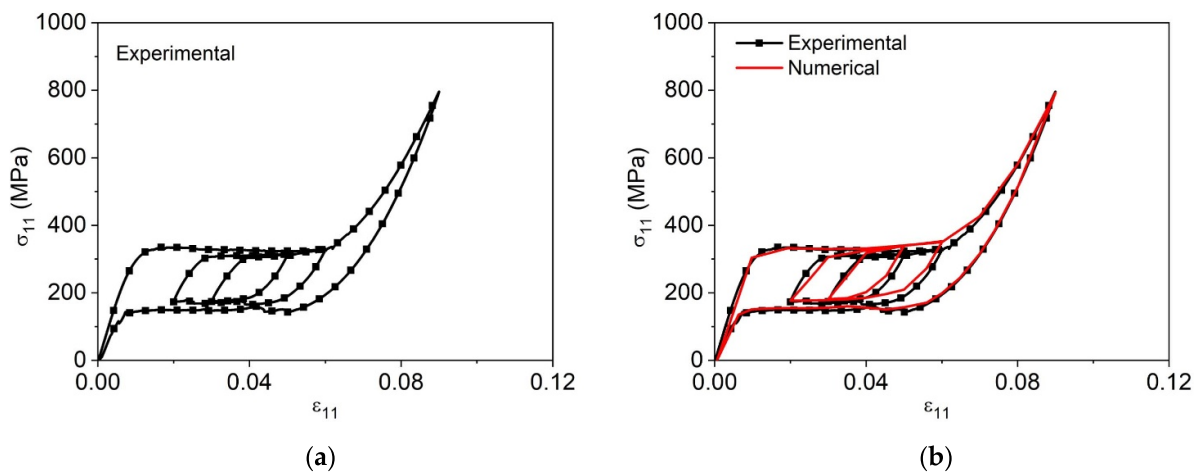


**Figure 15.** Pseudoelastic behavior of a NiTi wire during tensile tests, strain rate of  $0.5\% \text{ min}^{-1}$ . (a) Experimental result; (b) numerical-experimental comparative.

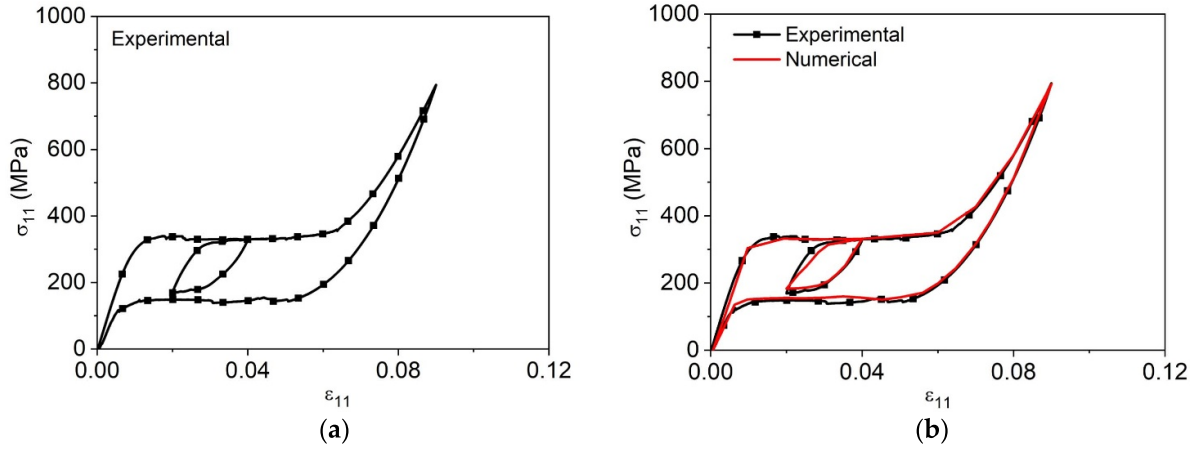


**Figure 16.** Pseudoelastic behavior of a NiTi wire during tensile tests, strain rate of  $1\% \text{ min}^{-1}$ . (a) Experimental result; (b) numerical-experimental comparative.

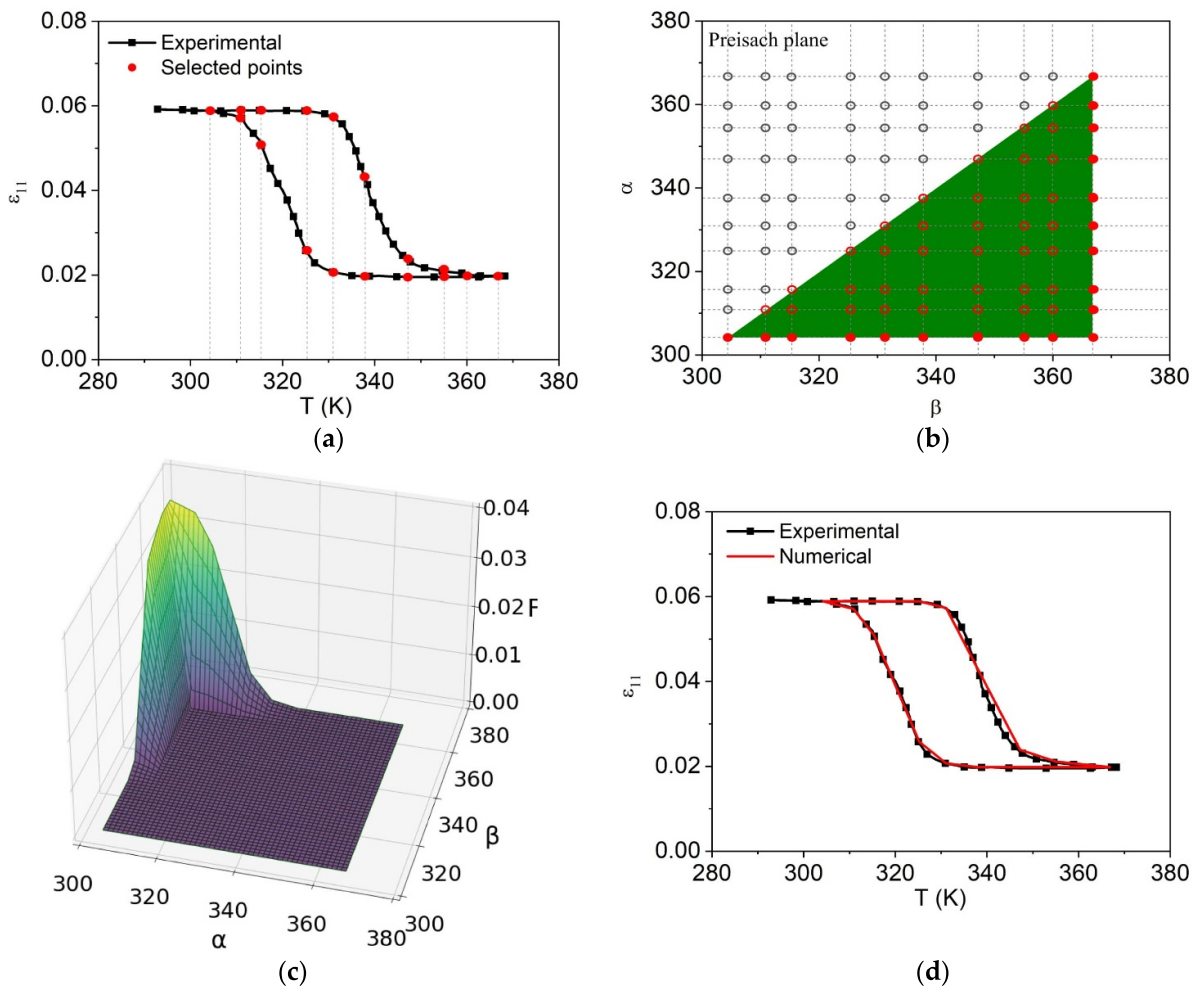


**Figure 17.** Thermal cyclic test under a constant uniaxial load based on the experimental test due to Qin *et al* [71]. (a) Selected points on the experimental curve used in the numerical implementation; (b) associated Preisach triangle; (c) Everett surface; (d) numerical-experimental comparison.

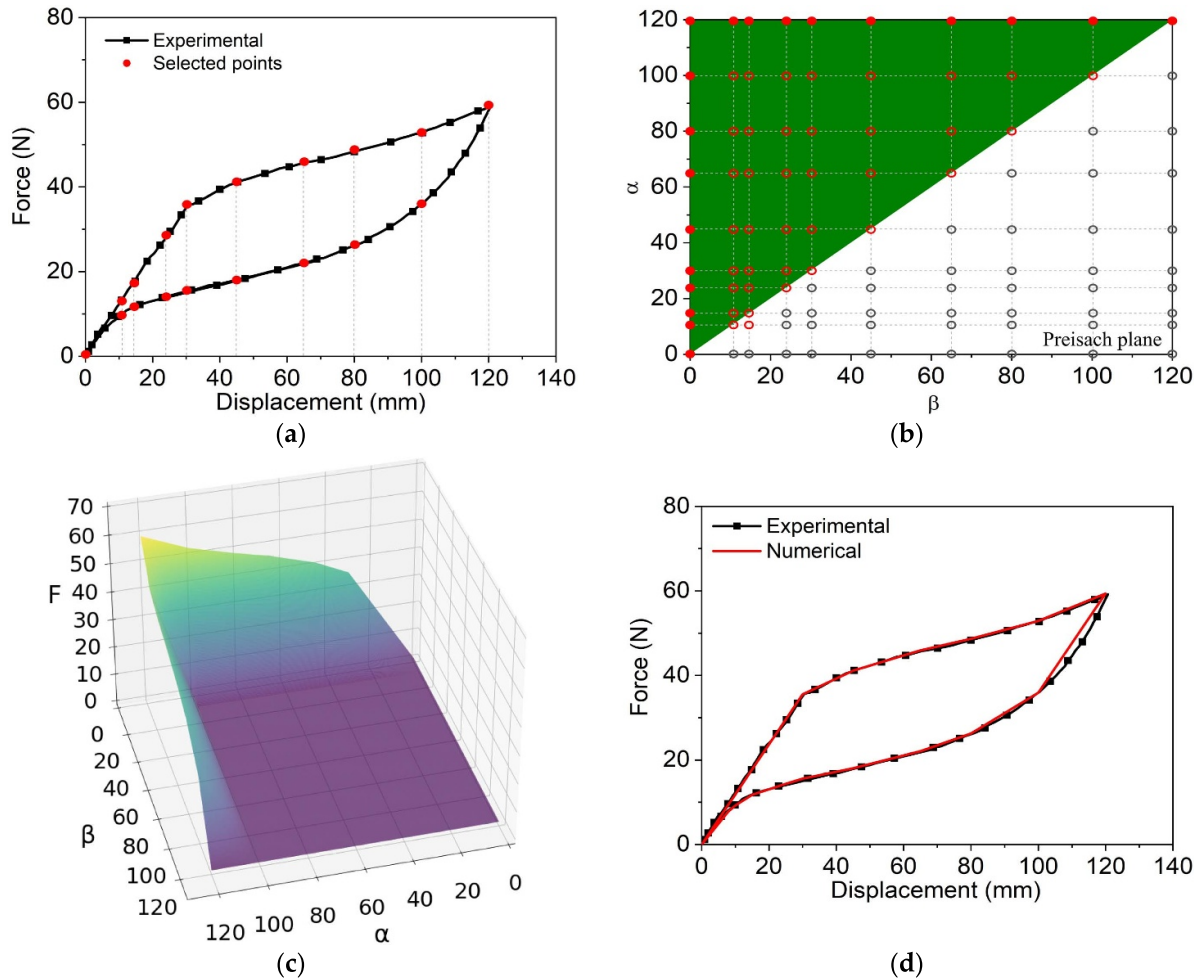


**Figure 18.** Experimental and numerical load-displacement curves based on the experimental test due to Savi *et al* [72]. (a) Selected points on the experimental curve used in the numerical implementation; (b) associated Preisach triangle; (c) Everett surface; (d) numerical-experimental comparison.

experimental results showing that the Preisach model captures the general behavior observed in experimental data, presenting a good agreement.

#### 4.4. SMA helical springs

The Preisach model is now employed to analyze the macroscopic behavior of a NiTi helical spring subjected to tensile tests considering experimental results presented by Savi *et al* [72]. Figure 18(a) shows the experimental force-displacement curve divided into nine regions and the respective selected points for the construction of the Everett function. It should be pointed out that now the input is the displacement while the output is the force. Figure 18(b) shows the associated Preisach triangle. Once again, the Everett function appears as an envelope of the Preisach triangle region since only experimental points of the outer loop are considered, as showed in figure 18(c). Figure 18(d) presents the numerical-experimental comparison where it should be pointed out a good agreement between results. It is noticeable that the Preisach model is capable to describe the pseudoelastic behavior of SMA springs

subjected to tensile tests, which means that force-displacement curves are also possible to be described.

In order to deal with internal subloops related to helical springs, experimental results proposed by Khan and Lagougas [61] are evaluated considering a NiTi spring subjected to compression tests with prescribed strain at an ambient temperature of 25 °C. Figure 19(a) shows the force-displacement curve considering twelve loading cycles, which include internal subloops, and the respective experimental points selected from twelve divisions of the experimental space. Figure 19(b) shows the correspondent Preisach triangle that is adjusted to contemplate the compression test. The Everett function is defined in the whole Preisach triangle domain as showed in figure 19(c). The numerical-experimental comparison is presented in figure 19(d) considering all the load cycles. Figure 19(e) presents the numerical-experimental comparison for the outer loop in order to facilitate the visualization of the proposed test. Once again, the model allows a close numerical-experimental agreement, demonstrating its ability to describe the SMA thermomechanical behavior of springs subjected to compressive loads.

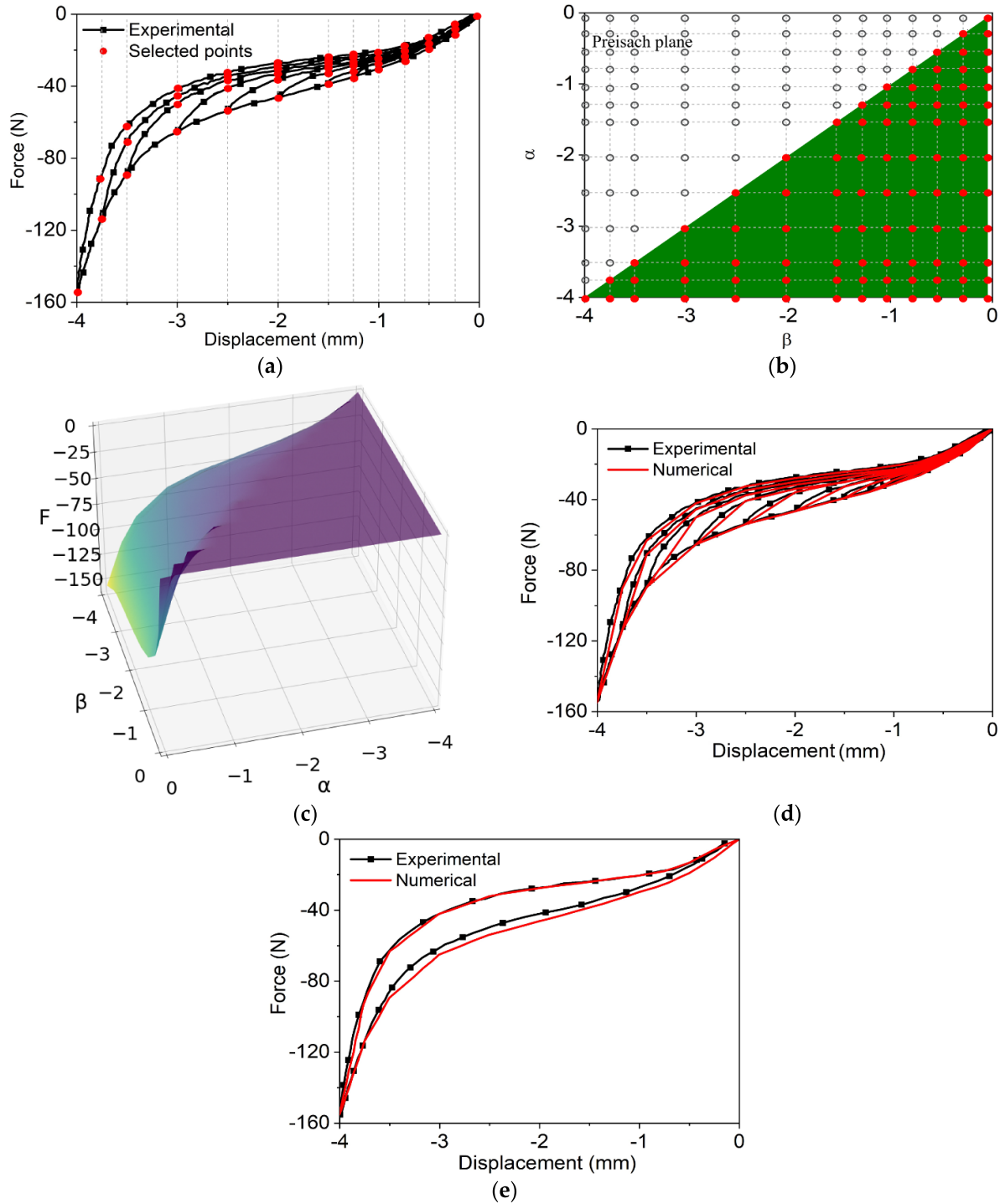


**Figure 19.** Numerical-experimental comparative based on the experimental test due to Khan and Lagoudas [61]. (a) Selected points on the experimental curve used in the numerical implementation; (b) associated Preisach triangle; (c) Everett surface; (d) numerical-experimental comparison considering all cycles; (e) numerical-experimental comparison considering the major cycle.

The tension-compression of a NiTi helical spring is now in focus considering the experimental tests proposed by Speicher *et al* [73] as reference. Figure 20(a) presents the experimental data, highlighting the proposed divisions and the experimental points. Figure 20(b) shows the Preisach triangles associated with both tension and compression. Once again,

only the experimental data of the external loops are considered, and the Everett function is an envelope of the Preisach triangles showed in figure 20(c). Figure 20(d) presents the numerical-experimental comparison indicating a good agreement, showing the model’s capability to represent the tension-compression of SMA springs.

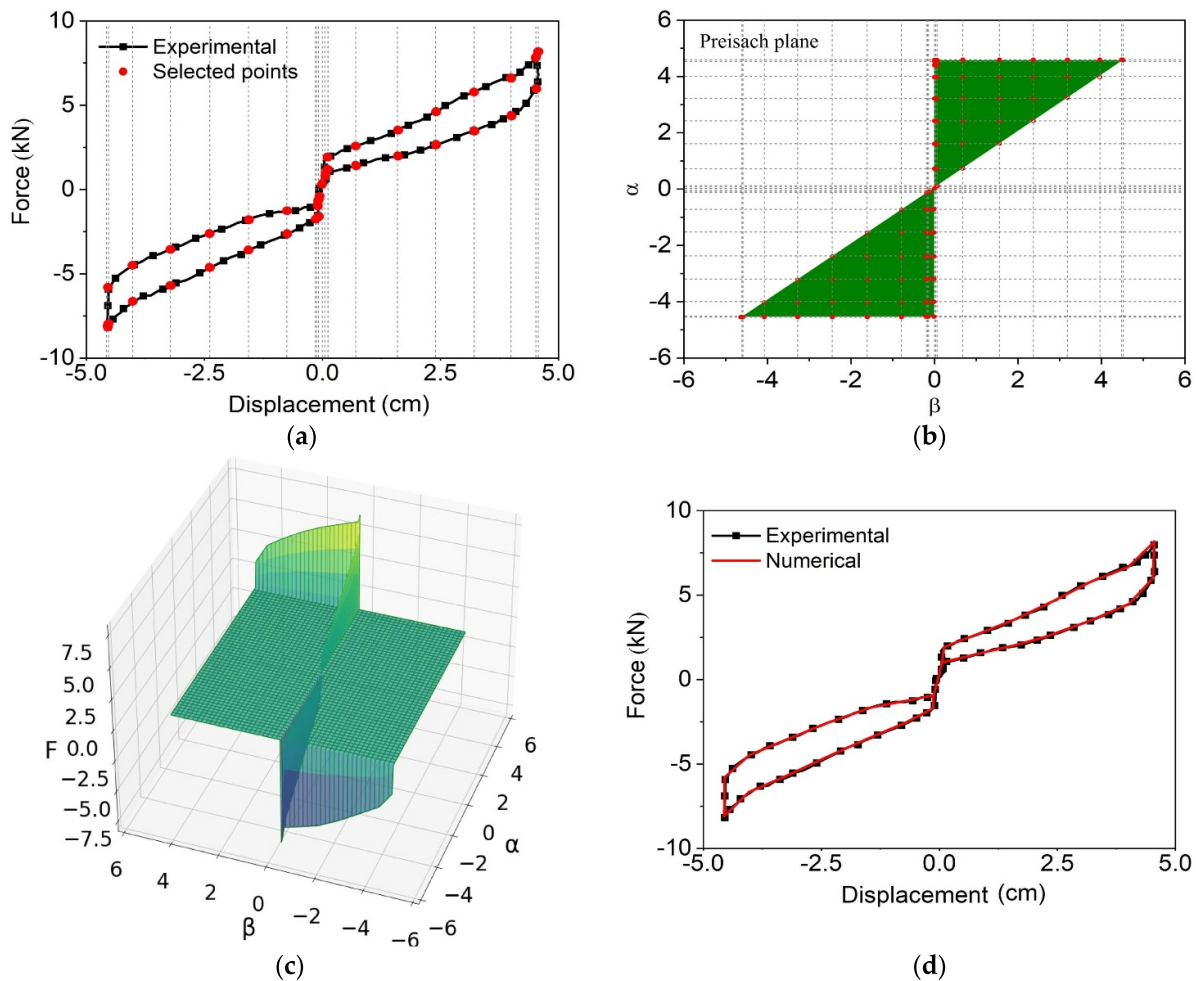


**Figure 20.** Numerical-experimental comparative based on the experimental test due to Speicher *et al* [73]. (a) Selected points on the experimental curve used in the numerical implementation; (b) associated Preisach triangle; (c) Everett surface; (d) numerical-experimental comparison.

## 5. Conclusions

This work investigates the thermomechanical description of SMAs using the Preisach model built from the Everett function that, in turn, is built from experimental data. Experimental tests are performed to identify some macroscopic characteristics of SMAs considering wire samples subjected to tensile tests. Different thermomechanical loads are of concern after a training process responsible for the phase transformation stabilization. In this regard, experimental tests provide different stress-strain curves related to internal subloops due to incomplete phase transformations. Numerical simulations are carried out and compared with the proposed experimental data, showing a good agreement. An important conclusion is that the thermomechanical behavior of SMAs can be described from a limit amount of information provided by experimental tests, being possible to extrapolate the behavior observed in experimental data based on the available information.

In addition, other tests are carried out based on different experimental data available in the literature considering strain-temperature of wires and force-displacement of helical springs. Once again, results show that the model responses are

in close agreement with experimental data. The model is able to capture the main features of the SMA thermomechanical behavior, properly describing stress-strain, strain-temperature and force-displacement curves. Besides, it should be pointed out that different tests can be reproduced with the same Everett function, which enlarges the model capability to describe macroscopic behaviors.

## Data availability statement

The data cannot be made publicly available upon publication because no suitable repository exists for hosting data in this field of study. The data that support the findings of this study are available upon reasonable request from the authors.

## Acknowledgments

The authors would like to acknowledge the support of the Brazilian Research Agencies CNPq (Conselho Nacional de Desenvolvimento Científico e Tecnológico), CAPES (Coordenação de Aperfeiçoamento de Pessoal de Nível

Superior) and FAPERJ (Fundação Carlos Chagas Filho de Amparo à Pesquisa do Estado do Rio de Janeiro). The support of the AFOSR (Air Force Office of Scientific Research) is also acknowledged.

### Conflict of interest

The authors declared no potential conflicts of interest with respect to the research, authorship, and/or publication of this article.

### ORCID iDs

Vanderson M Dornelas  <https://orcid.org/0000-0003-2784-3035>

Marcelo A Savi  <https://orcid.org/0000-0001-5454-5995>

### References

- [1] Otsuka K and Ren X 2005 Physical metallurgy of TiNi based shape memory alloys *Prog. Mater. Sci.* **50** 511–678
- [2] Lagoudas D C 2008 *Shape Memory Alloys, Modeling and Engineering Applications* (Springer)
- [3] Yamauchi K, Ohkata I, Tsuchiya K and Miyazaki S 2011 *Shape Memory and Superelastic Alloys: Applications and Technologies* (Woodhead Publishing)
- [4] Van Humbeeck J 1999 Non-medical applications of shape memory alloys *Mater. Sci. Eng. A* **273** 134–48
- [5] Machado L G and Savi M A 2003 Medical applications of shape memory alloys *Braz. J. Med. Biol. Res.* **36** 683–91
- [6] Janke L, Czaderski C, Motavalli M and Ruth J 2005 Applications of shape memory alloys in civil engineering structures—overview, limits and new ideas *Mater. Struct.* **38** 578–92
- [7] Isalgue A, Lovey F C, Terriault P, Martorell F, Torra R M and Torra V 2006 SMA for dampers in civil engineering *Mater. Trans.* **47** 682–90
- [8] Petrini L and Migliavacca F 2011 Biomedical applications of shape memory alloys *J. Metall.* **2011** 1–15
- [9] Mohd Jani J, Leary M, Subic A and Gibson M A 2013 A review of shape memory alloy research, applications and opportunities *Mater. Des.* **56** 1078–113
- [10] Lecce L and Concilio A 2015 *Shape Memory Alloy Engineering for Aerospace, Structural and Biomedical Applications* (Butterworth-Heinemann)
- [11] Chang W S and Araki Y 2016 Use of shape-memory alloys in construction: a critical interview *Proc. Inst. Civ. Eng.* **169** 87–95
- [12] Nematollahi M, Baghbaderani K S, Amerinatanzi A, Zamanian H and Elahinia M 2019 Application of NiTi in assistive and rehabilitation devices: a review *Bioengineering* **6** 37
- [13] Shreekrishna S, Nachimuthu R and Nair V S 2023 A review on shape memory alloys and their prominence in automotive technology *J. Intell. Mater. Syst. Struct.* **34** 499–524
- [14] Nair V S and Nachimuthu R 2022 The role of NiTi shape memory alloys in quality of life improvement through medical advancements: a comprehensive review *Proc. Inst. Mech. Eng. H* **236** 923–50
- [15] Saadat S, Salichs J, Noori M, Hou Z, Davoodi H, Baron I, Suzuki Y and Masuda A 2002 An overview of vibration and seismic applications of NiTi shape memory alloy *Smart Mater. Struct.* **11** 218
- [16] Leo D J 2007 *Engineering Analysis of Smart Material Systems* (Wiley)
- [17] Elahinia M H 2016 *Shape Memory Alloy Actuators: Design, Fabrication, and Experimental Evaluation* (Wiley)
- [18] Vignoli L L, Savi M A and El-Borgi S 2020 Nonlinear dynamics of earthquake-resistant structures using shape memory alloy composites *J. Intell. Mater. Syst. Struct.* **31** 771–87
- [19] Silva R S, Ritto T G and Savi M A 2021 Shape memory alloy couplers applied for torsional vibration attenuation of drill-string systems *J. Petrol. Sci. Eng.* **202** 108546
- [20] Paiva A and Savi M A 2006 An overview of constitutive models for shape memory alloys *Math. Probl. Eng.* **2006** 1–30
- [21] Khandelwal A and Buravalla V 2009 Models for shape memory alloy behavior: an overview of modeling approaches *Int. J. Struct. Changes Sol.* **1** 111–48
- [22] Cisse C, Zaki W and Zineb T B 2016 A review of constitutive models and modeling techniques for shape memory alloys *Int. J. Plast.* **76** 244–84
- [23] Cisse C, Zaki W and Zineb T B 2016 A review of modeling techniques for advanced effects in shape memory alloy behavior *Smart Mater. Struct.* **25** 1–36
- [24] Chowdhury P 2018 Frontiers of theoretical research on shape memory alloys: a general overview *Shape Mem. Superelasticity* **4** 26–40
- [25] Falk F 1980 Model free energy, mechanics, and thermodynamics of shape memory alloys *Acta Metall.* **28** 1773–80
- [26] Falk F 1983 One-dimensional model of shape memory alloys *Arch. Mech.* **35** 63–84
- [27] Tanaka K 1986 A thermomechanical sketch of shape memory effect: one-dimensional tensile behavior *Res. Mech.* **18** 251–63
- [28] Brinson L C 1993 One-dimensional constitutive behavior of shape memory alloys: thermomechanical derivation with non-constant material functions and redefined martensite internal variable *J. Intell. Mater. Syst. Struct.* **4** 229–42
- [29] Auricchio F and Sacco E 1997 A one-dimensional model for superelastic shape-memory alloys with different elastic properties between austenite and martensite *Int. J. Non Linear Mech.* **32** 1101–14
- [30] Savi M A, Paiva A, Baêta-Neves A P and Pacheco P M C L 2002 Phenomenological modeling and numerical simulation of shape memory: a thermo-plastic-phase transformation coupled model *J. Intell. Mater. Syst. Struct.* **3** 261–73
- [31] Paiva A, Savi M A, Braga A M B and Pacheco P M C L 2005 A constitutive model for shape memory alloys considering tensile-compressive asymmetry and plasticity *Int. J. Solids Struct.* **42** 3439–57
- [32] Adeodato A, Vignoli L L, Paiva A, Monteiro L L S, Pacheco P M C L and Savi M A 2022 A shape memory alloy constitutive model with polynomial phase transformation kinetics *Shape Mem. Superelasticity* **8** 1–18
- [33] Souza A C, Mamiya E N and Zouain N 1998 Three-dimensional model for solids undergoing stress-induced phase transformations *Eur. J. Mech. A* **17** 789–806
- [34] Popov P and Lagoudas D C 2007 A 3D constitutive model for shape memory alloys incorporating pseudoelasticity and detwinning of self-accommodated martensite *Int. J. Plast.* **23** 679–1720
- [35] Auricchio F, Reali A and Stefanelli U 2007 A three-dimensional model describing stress-induced solid phase transformation with permanent inelasticity *Int. J. Plast.* **23** 207–26
- [36] Oliveira S A, Savi M A and Zouain N 2016 A three dimensional description of shape memory alloy

- thermomechanical behavior including plasticity *J. Braz. Soc. Mech. Sci. Eng.* **38** 1451–72
- [37] Oliveira S A, Dornelas V M, Savi M A, Pacheco P M C L and Paiva A 2018 A phenomenological description of shape memory alloy transformation induced plasticity *Meccanica* **53** 2503–23
- [38] Chemisky Y, Hartl D J and Meraghni F 2018 Three-dimensional constitutive model for structural and functional fatigue of shape memory alloy actuators *Int. J. Fatigue* **112** 263–78
- [39] Phillips F R, Wheeler R W, Geltmacher A B and Lagoudas D C 2019 Evolution of internal damage during actuation fatigue in shape memory alloys *Int. J. Fatigue* **124** 315–27
- [40] Dornelas V M, Oliveira S A and Savi M A 2020 A macroscopic description of shape memory alloy functional fatigue *Int. J. Mech. Sci.* **170** 105345
- [41] Dornelas V M, Oliveira S A, Savi M A, Pacheco P M C L and de Souza L F G 2021 Fatigue on shape memory alloys: experimental observations and constitutive modeling *Int. J. Solids Struct.* **213** 1–24
- [42] Kuhnen K 2003 Modeling, identification and compensation of complex hysteretic nonlinearities: a modified Prandtl-Ishlinskii approach *Eur. J. Control* **9** 407–18
- [43] Al Janaideh M, Su C Y and Rakheja S 2008 Development of the rate-dependent Prandtl–Ishlinskii model for smart actuators *Smart Mater. Struct.* **173** 035026
- [44] Al Janaideh M, Rakheja S and Su C Y 2009 A generalized Prandtl–Ishlinskii model for characterizing the hysteresis and saturation nonlinearities of smart actuators *Smart Mater. Struct.* **18** 045001
- [45] Zakerzadeh M R and Sayyaadi H 2012 Experimental comparison of some phenomenological hysteresis models in characterizing hysteresis behavior of shape memory alloy actuators *J. Intell. Mater. Syst. Struct.* **23** 1287–309
- [46] Preisach F 1935 Über die magnetische Nachwirkung *Z. Phys.* **94** 277–302
- [47] Wang Y F, Su C Y, Hong H and Hu Y M 2007 Modeling and compensation for hysteresis of shape memory alloy actuators with the Preisach representation *IEEE (ICCAS)* pp 239–44
- [48] Mayergoz I D 1991 *Mathematical Models of Hysteresis* (Springer)
- [49] Song G, Zhao J, Zhou X and De Abreu-Garcia J A 2005 Tracking control of a piezoceramic actuator with hysteresis compensation using inverse Preisach model *IEEE/ASME Trans. Mechatronics* **10** 198–209
- [50] Dong Y, Hu H and Wang H 2014 Identification and experimental assessment of two-input Preisach model for coupling hysteresis in piezoelectric stack actuators *Sens. Actuators A* **220** 92–100
- [51] Xue Z, Li L, Ichchou M N and Li C 2017 Hysteresis and the nonlinear equivalent piezoelectric coefficient of MFCs for actuation *Chin. J. Aeronaut.* **30** 88–98
- [52] Adly A A, Mayergoz I D and Bergqvist A 1991 Preisach modeling of magnetostrictive hysteresis *J. Appl. Phys.* **69** 5777–9
- [53] Davino D, Natale C, Pirozzi S and Visone C 2004 Phenomenological dynamic model of a magnetostrictive actuator *Physica B* **343** 112–6
- [54] Li Z, Su C Y and Chai T 2013 Compensation of hysteresis nonlinearity in magnetostrictive actuators with inverse multiplicative structure for Preisach model *IEEE Trans. Autom. Sci. Eng.* **11** 613–9
- [55] Trapanese M, Franzitta V and Viola A 2014 A dynamic model for hysteresis in magnetostrictive devices *J. Appl. Phys.* **115** 17D141
- [56] Smith R C 2005 *Smart Material Systems: Model Development (Frontiers in Applied Mathematics)* (SIAM)
- [57] Hughes D C and Wen J T 1995 Preisach modeling and compensation for smart material hysteresis *Proc. SPIE* **2427** 50–64
- [58] Hughes D C and Wen J T 1997 Preisach modeling of piezoceramic and shape memory alloy hysteresis *Smart Mater. Struct.* **6** 287
- [59] Gorbet R B, Wang D W and Morris K A 1998 Preisach model identification of a two-wire SMA actuator *Proc. 1998 IEEE (ICRA)* vol 3 pp 2161–7
- [60] Mayergoz I D 2003 *Mathematical Models of Hysteresis and Their Applications* (Academic)
- [61] Khan M M and Lagoudas D C 2002 Modeling of shape memory alloy pseudoelastic spring elements using Preisach model for passive vibration isolation *Proc. SPIE* **4693** 336–47
- [62] Rao A and Srinivasa A R 2013 A two species thermodynamic Preisach model for the torsional response of shape memory alloy wires and springs under superelastic conditions *Int. J. Solid Struct.* **50** 887–98
- [63] Doraiswamy S, Rao A and Srinivasa A R 2011 Combining thermodynamic principles with Preisach models for superelastic shape memory alloy wires *Smart Mater. Struct.* **20** 085032
- [64] Rao A, Ruimi A and Srinivasa A R 2014 Internal loops in superelastic shape memory alloy wires under torsion—experiments and simulations/predictions *Int. J. Solids Struct.* **51** 4554–71
- [65] Ktena A, Fotiadis D I, Spanos P D, Berger A and Massalas C V 2002 Identification of 1D and 2D Preisach models for ferromagnets and shape memory alloys *Int. J. Eng. Sci.* **40** 2235–47
- [66] Matsuzaki Y, Funami K and Naito H 2002 Inner loops of pseudoelastic hysteresis of shape memory alloys: preisach approach *Proc. SPIE* **4699** 355–64
- [67] Liang H, Zeng C and Giraud-Audine C 2009 Modelling and simulation of shape memory alloys micro-actuator *Proc. 2009 IEEE (ICICIC)* pp 1405–8
- [68] Rao A and Srinivasa A R 2015 A three-species model for simulating torsional response of shape memory alloy components using thermodynamic principles and discrete Preisach models *Math. Mech. Solids* **20** 345–72
- [69] Chen Y, Shen X, Li J and Chen J 2019 Nonlinear hysteresis identification and compensation based on the discrete Preisach model of an aircraft morphing wing device manipulated by an SMA actuator *Chin. J. Aeronaut.* **32** 1040–50
- [70] Del Hoyo A B 2005 *Modelización de la histéresis magnética y su aplicación al cálculo numérico en máquinas eléctricas* (EUETIB-Departament d'Enginyeria Elèctrica)
- [71] Qin X, Zhang X, Yan X, Wang S, Zhang S, Guo C, Jiang J, Zhang B, Huang D and Qi M 2019 Structural and functional fatigue behavior of Ni<sub>49.8</sub>Ti<sub>50.2</sub> (at. %) wires under various maximum heating temperatures: experimental and modeling study *Mater. Des.* **178** 107842
- [72] Savi M A, Pacheco P M C, Garcia M S, Aguiar R A, De Souza L F G and Da Hora R B 2015 Nonlinear geometric influence on the mechanical behavior of shape memory alloy helical springs *Smart Mater. Struct.* **24** 035012
- [73] Speicher M, Hodgson D E, DesRoches R and Leon R T 2009 Shape memory alloy tension/compression device for seismic retrofit of buildings *J. Mater. Eng. Perform.* **18** 746–53